

Full angular dependence of the spin Hall and ordinary magnetoresistance in epitaxial antiferromagnetic NiO(001)/Pt thin films

L. Baldrati¹, A. Ross^{1,2}, T. Niizeki³, C. Schneider¹, R. Ramos³, J. Cramer^{1,2}, O. Gomonay¹, M. Filianina^{1,2}, T. Savchenko⁴, D. Heinze¹, A. Kleibert⁴, E. Saitoh^{3,5,6,7}, J. Sinova¹, M. Kläui^{1,2*}

¹*Institute of Physics, Johannes Gutenberg-University Mainz, 55128 Mainz, Germany*

²*Graduate School of Excellence Materials Science in Mainz, 55128 Mainz, Germany*

³*Advanced Institute for Materials Research, Tohoku University, Sendai 980-8577, Japan*

⁴*Swiss Light Source, Paul Scherrer Institute, 5232 Villigen PSI, Switzerland*

⁵*Institute for Materials Research, Tohoku University, Sendai 980-8577, Japan*

⁶*Advanced Science Research Center, Japan Atomic Energy Agency, Tokai 319-1195, Japan*

⁷*Center for Spintronics Research Network, Tohoku University, Sendai 980-8577, Japan*

**Electronic Mail: klaeui@uni-mainz.de*

ABSTRACT

We report the observation of the full angular dependence of the spin Hall magnetoresistance (SMR) in a thin film of epitaxial antiferromagnetic NiO, without any ferromagnetic element. The angular dependence of the magnetoresistance was measured in magnetic fields up to 11 T, using three orthogonal angular scans. We find that the total magnetoresistance has contributions arising both from SMR and ordinary magnetoresistance. Due to the particular NiO(001) orientation, and due to the fact that NiO(111) planes are easy-planes for the antiferromagnetic moment rotation, SMR is observable in all orthogonal planes. The onset of the SMR signal occurs between 1 and 3 T and no saturation is visible up to 11 T. The sign of the SMR is consistent with recent theoretical predictions and our results can be explained more quantitatively by a model considering the field-induced redistribution of S-domains, competing with the destressing energy arising from the interaction of the magnetostrictive NiO layer with the nonmagnetic MgO substrate. From the observed SMR ratio, we estimate the spin mixing conductance at the NiO/Pt interface to be greater than $1 \times 10^{14} \Omega^{-1} \text{ m}^{-2}$, comparable to early works on YIG/Pt systems. Our results highlight the presence of negative SMR in antiferromagnetic

thin films, confirming the existence of efficient spin transport and suggesting the possibility of an electrical detection of the Néel vector in this class of materials, even for thin films relevant for applications. Moreover, we show that a careful subtraction of the ordinary magnetoresistance contribution is crucial to correctly estimate the size of the SMR.

Manuscript

Antiferromagnets (AFMs) are materials with compensated magnetic sublattices, free from stray fields, robust against external magnetic perturbations and potentially operating at THz frequencies.^{1,2} In heavy metal/ferrimagnetic insulator (HM/FMI) bilayers such as Yttrium Iron Garnet (YIG)/Pt, the spin Hall magnetoresistance (SMR) has been first observed, i.e. a magnetoresistance effect caused by the interconversion between an electric current and a spin current, via the spin Hall effect (SHE) and inverse spin Hall effect (ISHE).³⁻⁵ In antiferromagnetic insulators, where no anisotropic magnetoresistance can be detected,⁶ SMR provides information on the orientation of the Néel vector,^{7,8} which otherwise can be only determined with X-ray magnetic linear dichroism (XMLD) at synchrotrons.⁹⁻¹¹ If SMR follows the same angular dependence as YIG/Pt bilayers, it is considered positive by convention,⁴ whilst negative when the maximum of the resistance is shifted by 90° as a function of the magnetic field **H**. This has been predicted in antiferromagnets,⁷ since the Néel vector **N** tends to align orthogonal to **H**, due to the higher magnetic susceptibility in this direction. At present, the sign of the SMR in antiferromagnets is not fully clarified. Both positive and negative SMR have been observed in HM/antiferromagnetic insulator(AFMI)/FM trilayers,¹²⁻¹⁵ where the spin backflow from the antiferromagnet and the FMI is detected. A non-monotonic behavior of the SMR as a function of the AFM thickness,^{12,14} and a change of sign as a function of temperature have been reported in AFMs,^{12-14,16} and in compensated ferrimagnets,¹⁷ suggesting a competition between positive and negative contributions, arising from the FMI and the AFMI, respectively. The SMR in bilayers of antiferromagnets/HM has been investigated only very

recently. Positive SMR was observed in bilayers of SrMnO_3/Pt ,¹⁸ and of $\text{Cr}_2\text{O}_3/\text{W}$,¹⁹ possibly due to a small canted/uncompensated magnetization \mathbf{M} .²⁰ A report on negative SMR in a $\text{NiO}(111)$ bulk crystal/Pt bilayer, where the magnetic field rotates in the NiO (111) easy plane only,²¹ in agreement with theoretical predictions,⁷ was published during the preparation of this work. However, at present, the full angular dependence of spin Hall magnetoresistance in an antiferromagnet has not been reported yet, nor it is clear how SMR can occur in epitaxial $\text{NiO}(001)$ thin films, the most stable NiO orientation,²² relevant for applications. In this paper, we fill these gaps, by showing the occurrence of SMR in a bilayer of Pt and epitaxial $\text{NiO}(001)$ thin films grown on $\text{MgO}(001)$ substrates by sputtering, fitting our results with a simple model based on the competition between Zeeman energy and destressing energy from the substrate.²³ Finally, from the measured data, we gauge the efficiency of the spin transport in antiferromagnetic thin films, by estimating the spin mixing conductance of the $\text{NiO}(001)/\text{Pt}$ interface.⁵

In ferromagnetic materials (FMs) presenting a net magnetization \mathbf{M} , the main component of the polarization of the spin current flowing along z (cf. Fig. 1b-d) is proportional to $\mathbf{M} \times (\mathbf{M} \times \boldsymbol{\mu}_s)$,⁵ where $\boldsymbol{\mu}_s$ is the polarization of the spin accumulation from the SHE. When $\mathbf{M} \parallel \boldsymbol{\mu}_s$, the spin current is reflected from the magnetic material,^{4,17} and the additional charge current induced by the conversion of the reflected spin current via the ISHE lowers the resistance. The spin current is instead absorbed by spin transfer torque if $\boldsymbol{\mu}_s \perp \mathbf{M}$, yielding a state of higher resistance in the HM. As a result, as the angle between the current and magnetic field is changed, a $\cos^2(\alpha)$ modulation of the resistance, following the definition of α in Fig. 1b, is obtained (positive SMR).⁴ By contrast, in antiferromagnets the magnetic moments follow the Néel vector \mathbf{N} , therefore the main component of the polarization of the spin current flowing along z is proportional to $\mathbf{N} \times (\mathbf{N} \times \boldsymbol{\mu}_s)$.^{4,7} Note that the configuration of lowest Zeeman energy is the one with $\mathbf{N} \perp \mathbf{H}$,²⁴ therefore the dependence of the SMR versus the field is shifted by 90° , yielding an expected $\sin^2(\alpha)$ dependence (negative SMR).

NiO is an easy-plane, collinear antiferromagnetic insulator with a band gap of 4 eV and a bulk Néel temperature of 523 K,^{25,26} representing an ideal model system to study SMR in AFMs. Above the Néel temperature, NiO exhibits a cubic rock salt structure, while the unit cell contracts along one of the four [111] directions in the bulk antiferromagnetic state.²⁶ Within each of these four magnetostrictive domains (T-domains), the spins are confined to ferromagnetic (111) planes, which in turn are antiferromagnetically ordered.^{26–28} The spins are relatively free to rotate to point in one of the three [11 $\bar{2}$] directions, leading to three possible independent spin domains (S-domains) within each of the T-domains. Like T-domains, S-domains also possess different strains of magnetoelastic origin. The magnetic structure of NiO, for a single S-domain, is shown schematically in Fig. 1a. With the application of an external field, the main mechanism of spin realignment is the motion of the AFM domain walls,^{24,26,28,29} which was reported to occur between <1 T and 7 T for bulk crystals.^{24,29–31}

The investigated NiO thin films of 90 nm thickness were grown on a (001)-oriented MgO substrate by means of radio frequency (RF) reactive magnetron sputtering. Epitaxial growth of NiO stems from the small lattice mismatch of ~1% between NiO ($a_{\text{NiO}} = 4.176 \text{ \AA}$) and MgO ($a_{\text{MgO}} = 4.212 \text{ \AA}$), both exhibiting a rock salt structure. The samples were grown in a sputtering system QAM4 from ULVAC, at a base pressure of 10^{-5} Pa . The MgO substrates were pre-annealed in vacuum at 800 °C for 2h. Subsequently, the NiO films were deposited from a Ni target in a steady Argon (15 sccm) and Oxygen (4.2 sccm) flow at 450 °C. Finally, a Pt top layer ($d_{\text{Pt}} = 7.5 \text{ nm}$) for the SMR experiment was deposited in-situ, after cooling down the samples to room temperature in vacuum. Epitaxial growth of the NiO(001) films was checked by X-ray diffraction and reciprocal space mapping, as detailed elsewhere.³²

The antiferromagnetic structure of a MgO/NiO(90 nm)/Pt(7.5 nm) sample was imaged by combining x-ray photoemission electron microscopy with the x-ray magnetic linear dichroism (XMLD) effect. The images were acquired at the Ni L₂ edge, using x-rays with linear vertical polarization and energy of 871.0 eV and 869.6 eV,¹⁰ and calculating the XMLD as the

difference of the images divided by the sum, while the x-ray beam was directed approximately along the 110 direction and at a grazing angle of 16° with respect to the surface of the sample. At $\mu_0H = 0$ T, our samples exhibit antiferromagnetic domains as shown in Fig. 1e, demonstrating the high quality of our NiO films and the presence of displaceable domain walls. Note that the XMLD contrast vanishes at 533 K, as expected based on the bulk Néel temperature, and no ferromagnetic contrast was seen in XMCD-PEEM measurements (see Supplementary information). Image distortions do not make XMLD-PEEM imaging possible at high applied magnetic fields so that one cannot probe the SMR by direct imaging.

As pointed out above, the application of an intense magnetic field to the NiO is known to induce a redistribution of AFM domains. In addition, we here propose a model taking into account the competition between elastic effects and the Zeeman energy, computed as $(\mathbf{N}\mathbf{H})^2/H_{\text{exch}}$, where H_{exch} parametrizes the exchange interaction between the magnetic sublattices. Below the Néel temperature, S-domains with different orientations of the Néel vector have different strains, due to the pronounced magnetoelastic interactions in NiO,³³ which are incompatible with the non-deformed nonmagnetic substrate and produce mechanical stresses in the sample. The macroscopic component of the stresses can be relaxed in the presence of a domain structure with zero average strain. We model this effect by introducing the destressing energy,^{6,23} which is proportional to $H_{\text{destr}}[\langle N_x^2 - N_y^2 \rangle^2 + 4\langle N_x N_y \rangle^2]$, where $\langle \rangle$ denotes the average. The value of the destressing field H_{destr} depends on the properties of the interface between NiO and the nonmagnetic substrate. Within this model the domain structure is described by the relative fraction of different domains which, assuming movable domain walls, could be considered as variables. Our calculations show that the effect of the external magnetic field, which removes the degeneracy of different S-domains, is partially screened by the domain redistribution. For in-plane field and a single (111) T-domain, the [2̄11] and [12̄1] S-domains compete, yielding a contribution into the longitudinal and transverse components of the resistance of the type:

$$\frac{\Delta R_{xx}(\alpha)}{\bar{R}} = \left(\frac{\Delta\rho}{\rho}\right) \frac{H^2}{H_{exch}H_{destr}} \sin^2(\alpha) \quad (1)$$

$$\frac{\Delta R_{xy}(\alpha)}{\bar{R}} = \left(\frac{\Delta\rho}{\rho}\right) \frac{H^2}{2H_{exch}H_{destr}} \sin(2\alpha) \quad (2)$$

where $\Delta\rho/\rho$ is the SMR value defined below (see Eq.(5)) and \bar{R} is the average resistance. The field applied in yz plane induces a redistribution of all three types of domains: $[\bar{2}11]$, $[1\bar{2}1]$ and $[11\bar{2}]$. In this case:

$$\frac{\Delta R_{xx}(\beta)}{\bar{R}} = \left(\frac{\Delta\rho}{\rho}\right) \frac{\sqrt{5}H^2}{2H_{exch}H_{destr}} \sin^2(\beta + \beta_{0,xx}) \quad (3)$$

$$\frac{\Delta R_{xy}(\beta)}{\bar{R}} = \left(\frac{\Delta\rho}{\rho}\right) \frac{\sqrt{10}H^2}{4H_{exch}H_{destr}} \sin[2(\beta + \beta_1)] \quad (4)$$

Where $\beta_{0,xx} \sim 26.8^\circ$ and $\beta_1 \sim 18.5^\circ$. A similar amplitude is also expected in the xz plane. Moreover, we can extract from the model a quadratic field dependence of the amplitude of SMR signal up to the monodomainization field $H_{MD} = \sqrt{2H_{exch}H_{destr}}$, at which all the unfavorable domains are swept out from the sample and the Néel vector is oriented perpendicular to the field direction. Above this field, the SMR signal saturates and does not depend on \mathbf{H} .

In order to check the validity of the model, the NiO/Pt bilayers were patterned into Hall bars, using electron beam lithography and ion beam etching. The Hall bar geometry is shown in Fig. 1f. The samples were installed in a variable temperature insert cryostat with a superconducting magnet, and static magnetic fields of up to 11 T were applied. The sample was rotated through the xy , yz and xz planes (Figs. 1b-d), by means of a piezoelectric rotator ANRv51RES from Attocube, operated in an open loop. While rotating the sample, a charge current from a Keithley 2400 was passed through the Hall bar and the transverse and longitudinal resistance were simultaneously captured with two Keithley 2182A nanovoltmeters. The sample was rotated clockwise by 180° degrees, then the field was reversed and the sample was rotated counter-clockwise to the initial position. The longitudinal and transverse resistance were calculated as the average sum and difference, respectively, of positive and negative currents. Drifts in the resistance occurring during the reversal of the field were corrected by summing a constant offset

to the backward part, in order to ensure the continuity of the resistance. Linear drifts due to a non-perfect temperature stabilization were corrected when detected. The sample temperature was maintained at 199.46 ± 0.02 K for all measurements, as probed by a Cernox-1050 sensor by Lakeshore.

The full angular dependence of the MR amplitude, for external fields $\mu_0\mathbf{H}$ up to 11 T, rotated in the xy, yz and xz planes, are shown in Fig. 2a-f. Note that there is a component of magnetoresistance in all the three planes. SMR is expected in our model to be observable in all the three planes, due to the fact that the (111) planes, where the rotation of the Néel vector is easier, are not parallel to the plane of the sample when the NiO orientation is (001). In YIG/NiO/Pt trilayers, the NiO has been shown to suppress the magnetic proximity effect in the Pt layer,¹² therefore we can exclude the presence of standard anisotropic magnetoresistance (AMR). Our data cannot be explained by the Hanle magnetoresistance, since a maximum of the Hanle resistance was measured in the xy plane for $\alpha = 0^\circ$ in the YIG/Pt system,³⁴ while we observe a minimum for the same angle and field of 11 T. At this high field and Pt thickness, however, a contribution of ordinary magnetoresistance (OMR) can arise in Pt.³⁵ In order to test the presence of other types of magnetoresistance, not related to the antiferromagnetic order, we grew and patterned a MgO//Pt(7.5 nm) control sample. The deposition condition and the device geometry were the same as the MgO//NiO/Pt sample. The resistances are identical within the error set by the thickness calibration for same nominal Pt thickness. The comparison between the MgO//Pt and the MgO//NiO/Pt, in the same experimental conditions at 11 T, is shown along all the three possible scan directions in fig. 3a-f. As can be seen, the longitudinal magnetoresistance of the MgO/Pt sample is always a fraction of the magnetoresistance of the MgO//NiO/Pt sample used for this study: 27% in the xy scan, 26% in the yz scan and 35% in the xz scan. By contrast, the Hall effect, shown in panels 3d,f has the same magnitude in both samples, as expected for identical Pt thickness and Hall bar geometry, highlighting the

comparability of the samples. So, we can identify the SMR contribution as the additional fraction of magnetoresistance in the NiO/Pt sample compared to the control MgO/Pt sample. The longitudinal (ΔR_{xx}) and transverse (ΔR_{xy}) resistance variations measured in the xy-plane scan were respectively fitted with a $\Delta R * \sin^2(\alpha + \alpha_{0,xx})$ and $\Delta R * \sin^2(\alpha + \alpha_{0,xy})$ functions (the fit is shown as continuous lines in Fig. 2a-b), where $\alpha_{0,xx}$ and $\alpha_{0,xy}$ are constants. The small differences of the offsets $\alpha_{0,xx} = 6^\circ \pm 2^\circ$ and $\alpha_{0,xy} = -40^\circ \pm 2^\circ$, to the respectively expected values of 0° and -45° , are likely due to a non-corrected misalignment of the direction of the current, while their difference $\alpha_{0,xx} - \alpha_{0,xy} = 46 \pm 3^\circ$ is in agreement to what is expected for SMR. The data shows a negative sign of the SMR within the xy plane, i.e. the longitudinal resistance of the Pt is highest when the external field $\mathbf{H} \parallel \mu_s$, and minimized for $\mathbf{H} \perp \mu_s$. This is in contrast to the expectation in ferromagnets (FMs) exhibiting a net magnetization \mathbf{M} , but in agreement with theoretical predictions for antiferromagnets,⁷ with the negative sign of the SMR found in YIG/NiO/Pt trilayers^{12–14} and in NiO(111)/Pt single bulk crystals.²¹ This implies that the SMR in our system results from a component of the Néel vector perpendicular to the field and supports the validity of our model.

For the yz and xz planes, the transverse signal is dominated by the ordinary Hall effect of the Pt top layer, which is linear with the field and follows a $-\cos(\theta + \theta_{0,Hall})$ functional angular dependence. By correcting the offset in order to set $\theta_{0,Hall} = 0^\circ$, and applying the same correction to the transverse and longitudinal data, we find that the longitudinal resistance is modulated with a $\Delta R * \sin^2(\beta + \beta_{0,xx})$ dependence in the yz plane, where surprisingly $\beta_{0,xx} = 31^\circ \pm 3^\circ$ has a finite value. By contrast, the dependence in the xz plane is $\Delta R * \sin^2(\gamma + \gamma_{0,xx})$, with $\gamma_{0,xx} = 1 \pm 2^\circ$. As pointed out above, a contribution from ordinary magnetoresistance is present in Pt at high magnetic fields. This contribution is less than 35% of the total magnetoresistance measured in the NiO/Pt at 11 T in all the three planes under study, as determined by the comparison to the MgO/Pt control sample. Based on the ratio between OMR and SMR at 11 T

in the three planes, we subtracted the same relative contribution to the field dependence. We can therefore fit the magnetoresistance data, after removing the OMR contribution, with our model. The SMR amplitude in the three planes is shown in Fig. 4, together with the quadratic fit from the model. The longitudinal and transverse SMR amplitudes increase with the field, showing no saturation, and are in good agreement with each other and with the model, if the geometric scaling factor of 8.67, calculated as the ratio between the length and width of the Hall bar, is taken into account. Note that, according to equations (1) and (2), the longitudinal and transverse components are shifted by 45° , which agrees well with the measurements in Fig. 2a,b, as discussed above. Moreover, the experimental dependences shown in Fig. 2c,d and the fit from the experiments yields a value of $\beta_{0,xx} = 31^\circ \pm 3^\circ$, matching well the value of $\beta_{0,xx} \sim 26.8^\circ$ predicted in Eqs. (3) and (4). The different value of the fitted amplitude and of the phase between the xz and yz scans cannot be explained by our simple model. This difference may arise from pinning of the domain walls, which may favor the propagation along specific directions, or may be related to the presence of different antiferromagnetic T-domains, which may lead to a different response to an external magnetic fields as a function of the plane where this field is applied.

In our experiments, no saturation of the signal up to 11 T is observed. The absence of saturation at 11 T is probably related to the non-favorable geometry of the nickel oxide: the highest angle between the $\{111\}$ planes and the xy plane occurs along the [100] directions, i.e. at $\sim 54.7^\circ$. If we consider the projection and the saturation fields of Hoogeboom et al.²¹ (6 T) for single crystal, we expect a saturation field of 10.4 T, at the limit of the field range used. Moreover, recently a saturation field of 13 T in NiO(111) thin films was claimed.³⁶

Finally, from the measured SMR ratio $\Delta\rho/\rho$ at 11 T, calculated as the difference between the total MR ratio and the OMR in the control sample, we can set a lower limit for the spin mixing conductance by using the formula from the model based on spin diffusion theory by Chen et al.⁵

$$\frac{\Delta\rho}{\rho} = \theta_{SH}^2 \frac{\lambda}{d_{Pt}} Re \left(\frac{2\lambda G_{\uparrow\downarrow} \tanh^2 \left(\frac{d_{Pt}}{2\lambda} \right)}{\sigma + 2\lambda G_{\uparrow\downarrow} \coth \left(\frac{d_{Pt}}{\lambda} \right)} \right) \quad (5)$$

where λ is the spin relaxation length in the Pt (1.1 nm),³⁷ σ is the measured Pt conductivity ($5.5 \times 10^6 \Omega^{-1} \text{ m}^{-1}$), θ_{SH} is the spin Hall angle of the Pt (0.08),³⁷ and d_{Pt} is the Pt thickness (7.5 nm). By using these values, we obtain the lower limit for the spin mixing conductance at the NiO/Pt interface to be $G_{\uparrow\downarrow} \sim 1 \times 10^{14} \Omega^{-1} \text{ m}^{-2}$. This value is compatible to what was obtained in YIG/Pt,⁴ and it fits well with the order of magnitude of recent theoretical predictions,⁷ while it is lower than what was reported by Han et al.¹⁸ in Pt/SrMnO₃. However, from the data by Hoogeboom et al.²¹ in single crystals of NiO(111)/Pt, where a strong dependence on the interface treatment was found, and considering that 11 T are not sufficient to saturate the signal, we expect that the spin mixing conductance can be further optimized.³⁸

In conclusion, we report on a negative spin Hall magnetoresistance in NiO(001)/Pt epitaxial thin films grown on MgO(001) substrates. The measured symmetry of the spin Hall magnetoresistance is consistent with theoretical expectations.⁷ Our results demonstrate that the SMR in epitaxial thin films is measurable even in the presence of clamping effect from a substrate and for crystal orientations not favorable for the magnetic moment reorientation in an easy plane. When the NiO(111) easy plane is not parallel to the surface of the NiO film, the redistribution of the magnetic domains as a function of the field is found to be non-trivial. We propose a simple model to determine the fraction of different S- domains, by taking into account the competition between Zeeman and destressing energy, for a thin film experiencing a clamping effect from the substrate. The model explains the quadratic field dependence of the SMR ratio, the negative sign of the SMR observed in the xy plane and the offset of the SMR in the yz plane, which is $\beta_{0,xx} = 31^\circ \pm 3^\circ$. From the observed SMR ratio, we estimate a spin mixing conductance greater than $1 \times 10^{14} \Omega^{-1} \text{ m}^{-2}$, close to the one observed in YIG/Pt.⁴ Our results confirm the potential of spin transport in antiferromagnetic insulating thin films, which are relevant for applications and represent a step toward the all-electrical detection of the magnetic

moments in this class of materials. A careful subtraction of ordinary magnetoresistance in the Pt layer is crucial to correctly estimate the SMR, which also has to be considered in view of applications and using transport measurements to identify the Néel vector orientation of the antiferromagnet.

Supplementary material

See Supplementary material for XMCD- and XMLD-PEEM characterization of the NiO magnetic properties and magnetoresistance measurements of a MgO/Pt control sample.

Acknowledgements

This work was supported by Deutsche Forschungsgemeinschaft (DFG) SPP 1538 “Spin Caloric Transport,” the Graduate School of Excellence Materials Science in Mainz (MAINZ), and the EU project INSPIN (FP7-ICT-2013-X 612759). The authors acknowledge the support of SpinNet (DAAD Spintronics network, project number 56268455), MaHoJeRo (DAAD Spintronics network, project number 57334897), the SNSF (project number 200021_160186), and the DFG (SFB TRR 173 SPIN+X). O.G. and J.S. acknowledge the Alexander von Humboldt Foundation and the ERC Synergy Grant SC2 (No. 610115). This work was supported by ERATO “Spin Quantum Rectification Project” (Grant No. JPMJER1402) and Grant-in-Aid for Scientific Research on Innovative Area, “Nano Spin Conversion Science” (Grant No. JP26103005) from JSPS KAKENHI, Japan, and the NEC Corporation. Part of this work was performed at the Surface/Interface:Microscopy (SIM) beamline of the Swiss Light Source, Paul Scherrer Institut, Villigen, Switzerland. M.K. thanks ICC-IMR at Tohoku University for their hospitality during a visiting researcher stay at the Institute for Materials Research. The authors acknowledge useful scientific discussion with G. E. W. Bauer, R. Lebrun, D.-S. Han and K. Lee, as well as skillful technical support from J. Henrizi.

References

¹ T. Jungwirth, X. Marti, P. Wadley, and J. Wunderlich, *Nat. Nanotechnol.* **11**, 231 (2016).

² V. Baltz, A. Manchon, M. Tsoi, T. Moriyama, T. Ono, and Y. Tserkovnyak, *arXiv:1606.04284* 1 (2016).

³ J. Sinova, S.O. Valenzuela, J. Wunderlich, C.H. Back, and T. Jungwirth, *Rev. Mod. Phys.* **87**, 1213 (2015).

⁴ H. Nakayama, M. Althammer, Y.T. Chen, K. Uchida, Y. Kajiwara, D. Kikuchi, T. Ohtani, S. Geprägs, M. Opel, S. Takahashi, R. Gross, G.E.W. Bauer, S.T.B. Goennenwein, and E. Saitoh, *Phys. Rev. Lett.* **110**, 206601 (2013).

⁵ Y.-T. Chen, S. Takahashi, H. Nakayama, M. Althammer, S.T.B. Goennenwein, E. Saitoh, and G.E.W. Bauer, *Phys. Rev. B* **87**, 144411 (2013).

⁶ E. V. Gomonaj and V.M. Loktev, *Phys. Rev. B* **64**, 064406 (2001).

⁷ A. Manchon, *Phys. Status Solidi - Rapid Res. Lett.* **11**, 1600409 (2017).

⁸ H. Wang, D. Hou, Z. Qiu, T. Kikkawa, E. Saitoh, and X. Jin, *J. Appl. Phys.* **122**, 083907 (2017).

⁹ H. Ohldag, A. Scholl, F. Nolting, S. Anders, F.U. Hillebrecht, and J. Stöhr, *Phys. Rev. Lett.* **86**, 2878 (2001).

¹⁰ K. Arai, T. Okuda, A. Tanaka, M. Kotsugi, K. Fukumoto, T. Ohkochi, T. Nakamura, T. Matsushita, T. Muro, M. Oura, Y. Senba, H. Ohashi, A. Kakizaki, C. Mitsumata, and T. Kinoshita, *Phys. Rev. B* **85**, 104418 (2012).

¹¹ G. Van Der Laan, N.D. Telling, A. Potenza, S.S. Dhesi, and E. Arenholz, *Phys. Rev. B - Condens. Matter Mater. Phys.* **83**, 064409 (2011).

¹² T. Shang, Q.F. Zhan, H.L. Yang, Z.H. Zuo, Y.L. Xie, L.P. Liu, S.L. Zhang, Y. Zhang, H.H. Li, B.M. Wang, Y.H. Wu, S. Zhang, and R.W. Li, *Appl. Phys. Lett.* **109**, 032410 (2016).

¹³ D. Hou, Z. Qiu, J. Barker, K. Sato, K. Yamamoto, S. Vélez, J.M. Gomez-Perez, L.E. Hueso, F. Casanova, and E. Saitoh, *Phys. Rev. Lett.* **118**, 147202 (2017).

¹⁴ W. Lin and C.L. Chien, Phys. Rev. Lett. **118**, 067202 (2017).

¹⁵ Y.M. Hung, C. Hahn, H. Chang, M. Wu, H. Ohldag, and A.D. Kent, AIP Adv. **7**, 055903 (2017).

¹⁶ T. Shang, H.L. Yang, Q.F. Zhan, Z.H. Zuo, Y.L. Xie, L.P. Liu, S.L. Zhang, Y. Zhang, H.H. Li, B.M. Wang, Y.H. Wu, S. Zhang, and R.-W. Li, J. Appl. Phys. **120**, 133901 (2016).

¹⁷ K. Ganzhorn, J. Barker, R. Schlitz, B.A. Piot, K. Ollefs, F. Guillou, F. Wilhelm, A. Rogalev, M. Opel, M. Althammer, S. Geprägs, H. Huebl, R. Gross, G.E.W. Bauer, and S.T.B. Goennenwein, Phys. Rev. B **94**, 094401 (2016).

¹⁸ J.H. Han, C. Song, F. Li, Y.Y. Wang, G.Y. Wang, Q.H. Yang, and F. Pan, Phys. Rev. B **90**, 144431 (2014).

¹⁹ Y. Ji, J. Miao, K.K. Meng, Z.Y. Ren, B.W. Dong, X.G. Xu, Y. Wu, and Y. Jiang, Appl. Phys. Lett. **110**, 262401 (2017).

²⁰ O. Gomonay, S. Kondovych, and V. Loktev, J. Magn. Magn. Mater. **354**, 125 (2014).

²¹ G.R. Hoogeboom, A. Aqeel, T. Kuschel, T.T.M. Palstra, and B.J. van Wees, Appl. Phys. Lett. **111**, 052409 (2017).

²² O.L. Warren and P.A. Thiel, J. Chem. Phys. **100**, 659 (1994).

²³ H. Gomonay and V.M. Loktev, J. Phys. Condens. Matter **14**, 3959 (2002).

²⁴ J. Milano and M. Grimsditch, Phys. Rev. B - Condens. Matter Mater. Phys. **81**, 094415 (2010).

²⁵ R.J. Powell and W.E. Spicer, Phys. Rev. B **2**, 2182 (1970).

²⁶ W.L. Roth, J. Appl. Phys. **31**, 2000 (1960).

²⁷ G.A. Slack, J. Appl. Phys. **31**, 1571 (1960).

²⁸ W.L. Roth and G.A. Slack, J. Appl. Phys. **31**, S352 (1960).

²⁹ J. Milano, L.B. Steren, and M. Grimsditch, Phys. Rev. Lett. **93**, 077601 (2004).

³⁰ F.L.A. Machado, P.R.T. Ribeiro, J. Holanda, R.L. Rodríguez-Suárez, A. Azevedo, and S.M. Rezende, Phys. Rev. B **95**, 104418 (2017).

³¹ A.N. Bogdanov, A. V. Zhuravlev, and U.K. Rößler, Phys. Rev. B **75**, 094425 (2007).

³² L. Baldrati, C. Schneider, T. Niizeki, R. Ramos, J. Cramer, A. Ross, E. Saitoh, and M. Kläui, Manuscript in Preparation (2017).

³³ T. Yamada, J. Phys. Soc. Japan **21**, 664 (1966).

³⁴ S. Vélez, V.N. Golovach, A. Bedoya-Pinto, M. Isasa, E. Sagasta, M. Abadia, C. Rogero, L.E. Hueso, F.S. Bergeret, and F. Casanova, Phys. Rev. Lett. **116**, 016603 (2016).

³⁵ M. Isasa, S. Vélez, E. Sagasta, A. Bedoya-Pinto, N. Dix, F. Sánchez, L.E. Hueso, J. Fontcuberta, and F. Casanova, Phys. Rev. Appl. **6**, 034007 (2016).

³⁶ J. Fischer, O. Gomonay, R. Schlitz, K. Ganzhorn, N. Vlietstra, M. Althammer, H. Huebl, M. Opel, R. Gross, S.T.B. Goennenwein, and S. Gepraegs, arXiv:1709.04158 (2017).

³⁷ N. Vlietstra, J. Shan, V. Castel, J. Ben Youssef, G.E.W. Bauer, and B.J. Van Wees, Appl. Phys. Lett. **103**, 032401 (2013).

³⁸ Note that the spin mixing conductance of $10^{18} \Omega^{-1} m^{-2}$, claimed in single crystalline NiO/Pt, is overestimated due to a miscalculation (G. R. Hoogeboom, private communication).

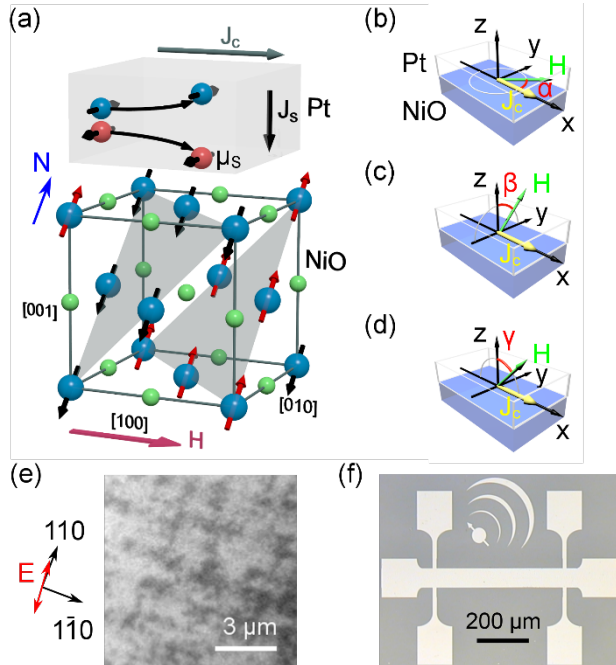


Fig. 1: (a) Measurement scheme of Spin Hall magnetoresistance (SMR) in MgO/NiO(001)/Pt.

A charge current J_c flows in the Pt layer, yielding a transverse spin current J_s in the NiO, via the spin Hall effect. Depending on the relative orientation between the Néel vector \mathbf{N} (blue arrow) and the current-induced spin polarization μ_s , the spin current is converted into an additional charge current by the inverse spin Hall effect, yielding the SMR. The spin structure of one of the twelve possible $(11\bar{2})$ S-domains of the NiO is shown, as well as the (111) easy plane. (b)-(d) Geometry of xy-, yz- and xz planes, and definition of the angles α , β and γ . (e) XMLD image showing the antiferromagnetic domains in NiO at $\mu_0 H = 0$ T. The arrows indicate the orientation of the crystalline axes of the sample and of the electric field E of the X-ray beam. (f) Optical microscope image of the Hall bar design used for the magnetoresistance experiments.

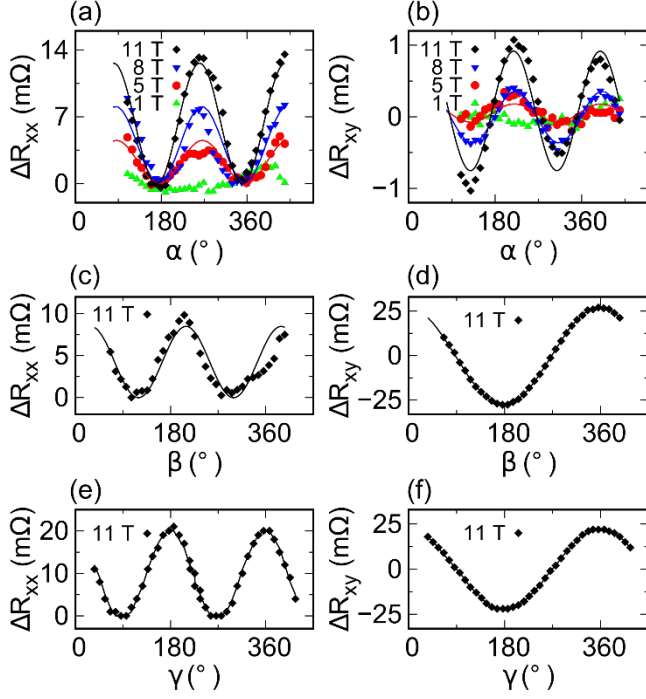


Fig. 2: Longitudinal ($\Delta R_{xx} = R_{xx}(\theta) - \min(R_{xx})$) and transverse ($\Delta R_{xy} = R_{xy}(\theta) - \bar{R}_{xy}$) angular dependence of the resistance variation of NiO/Pt bilayers at 199.46 ± 0.02 K, where \bar{R} is the angle-averaged resistance. (a)-(b) Longitudinal resistance variation ΔR_{xx} and transverse resistance variation ΔR_{xy} in the xy-plane, as a function of the in-plane angle α for applied field of 1, 5, 8 and 11 T. (c)-(d) ΔR_{xx} and ΔR_{xy} in the yz plane, as a function of the out-of-plane angle β . Note the predominance of the Hall effect in the transverse resistance. (e)-(f) ΔR_{xx} and ΔR_{xy} in the xz plane, as a function of the out-of-plane angle γ . The continuous lines show the $\Delta R^* \sin^2(\theta + \theta_0)$ fit of the data, except for the ΔR_{xy} data in the xz and yz planes, which is fitted by $\Delta R^* \cos(\theta + \theta_0)$.

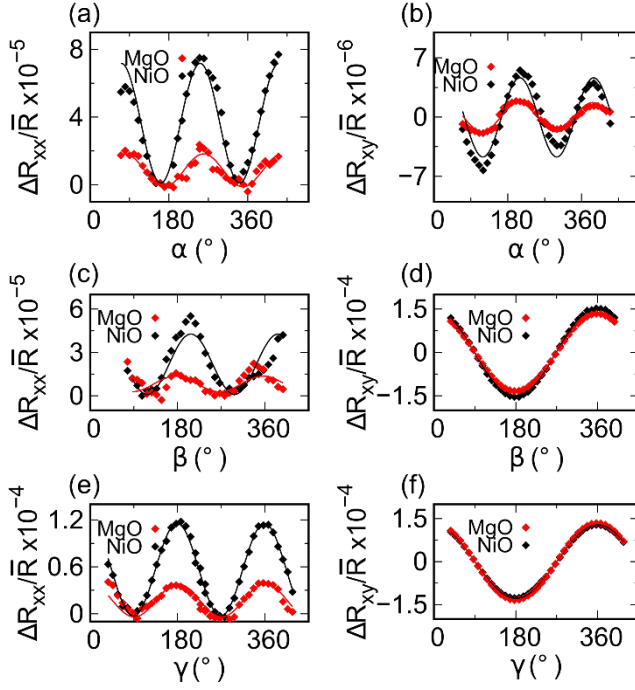


Fig. 3: Comparison between the longitudinal and transverse angular dependence of the resistance variation in MgO/NiO(90 nm)/Pt(7.5 nm), shown by black dots, and a MgO//Pt(7.5 nm) sample, shown by red dots, in an applied field at $\mu_0 H = 11$ T at 199.46 ± 0.02 K. The resistances are measured by rotating the samples in (a-b) xy plane, (c-d) yz plane, (e-f) xz plane. Note that the longitudinal and transverse resistance are significantly different (panels a,b,c,e), while the Hall effect in the out of plane scans is the same (panels d,f).

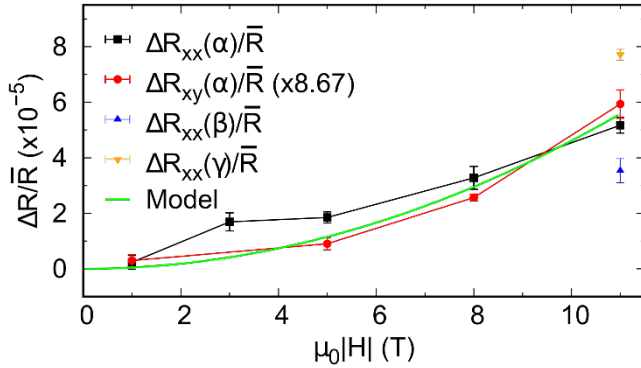


Fig. 4: Amplitude ΔR of the longitudinal and transverse resistance variation obtained by the $\Delta R * \sin^2(\theta + \theta_0)$ fit of the data for different magnetic field amplitude and divided by the angle-averaged resistance \bar{R} . The data were acquired in the xy, xz and yz plane scans at 199.46 ± 0.02 K and are compared to the theoretical model (green solid line). No saturation is observed in the field range used.